*Meteoritics & Planetary Science* 37, 1197–1207 (2002)
Available online at http://www.uark.edu/meteor

# Crustal properties of Mercury by morphometric analysis of multi-ring basins on the Moon and Mars

LARAMIE V. POTTS[1,3]*, RALPH R. B. VON FRESE[1,2] AND C. K. SHUM[1,3]

[1]Laboratory for Space Geodesy and Remote Sensing Research, The Ohio State University, Columbus, Ohio 43210, USA
[2]Department of Geological Sciences, The Ohio State University, Columbus, Ohio 43210, USA
[3]Department of Civil and Environmental Engineering and Geodetic Science, The Ohio State University, Columbus, Ohio 43210, USA
*Correspondence author's e-mail address: potts.3@osu.edu

*(Received 2002 January 11; accepted in revised form 2002 May 17)*
*(Presented at the Workshop on Mercury, The Field Museum, Chicago, Illinois, 2001 October 4–5)*

**Abstract**–We use satellite altitude free-air and terrain gravity correlations to differentiate regional variations in crustal viscosity and transient cavity diameters of impact basins on the Moon and Mars that we combine with surface roughness for a rheological assessment of the crust of Mercury. For the Moon and Mars, we separate the free-air anomalies into terrain-correlated and terrain-decorrelated components using the spectral properties of the free-air and computed terrain gravity effects. Adjusting the terrain effects for the terrain-correlated anomalies yields compensated terrain effects that we evaluate for crustal thickness variations of the impact basins. We interpret the terrain-correlated anomalies for uncompensated elements of the crustal thickness variations that we find are strongly correlated with the distribution of basin rings from photogeologic analyses. Hence, we estimate the transient cavity diameter from the innermost diameter of the gravity-inferred rings. Comparing these diameters with the related crustal thickness estimates clearly differentiates regional variations in the crustal rheologies. For the Moon, the analysis points to a farside crust that was significantly more rigid than the nearside crust during bombardment time. For Mars, the growth in transient cavity diameters with apparent crustal age also reflects increased viscosity due to crustal cooling. These results are also consistent with local estimates of surface roughness developed from the root-mean-squared topography over 64 × 64° patches centered on the basins. Hence for Mercury where gravity observations are lacking, rheological inferences on its crust may result from comparing photometric estimates of transient cavity diameter and local surface roughness with the lunar and martian estimates. These results for the Beethoven Basin, a typical multi-ring impact feature of Mercury, suggest that the viscosity of the mercurian crust was relatively great during bombardment time. This enhanced rigidity, despite crustal temperatures that were probably much hotter than those of the Moon and Mars, may reflect an extremely dry crust for Mercury in its early development.

## INTRODUCTION

Insight on the mechanical attributes of planetary lithospheres has been provided by substrate rheology inferred from surface topography (*e.g.*, Galdikas, 1999) and the direct proportionality between crustal viscosity and size of the transient cavity of an impact basin (*e.g.*, Melosh, 1982; Spudis, 1993). We investigate these relationships for the multi-ring impact basins of the Moon and Mars using free-air and terrain gravity correlations. We also consider their use for inferring the rheological attributes of the crust of Mercury where gravity observations are lacking.

For the Moon, altimetry data from the Clementine mission (Nozette *et al.*, 1994) reveal a dichotomy in surface roughness (Lucey *et al.*, 1994) that reflects early differentiation processes (Stevenson, 1980) where the higher thermal gradient in the nearside crust (Solomon *et al.*, 1982) produced smoother topography than on the cooler and more viscous farside. Gravity data from the Lunar Prospector and earlier missions (Binder, 1998) in combination with computed gravity effects of the lunar topography also show the nearside and farside dichotomy in surface roughness to be complemented directly by crustal thickness and strength variations (Potts and von Frese, 2001b) to further support the differentiation hypothesis for the primordial Moon (Stevenson, 1980).

For Mars, altimetry data from the *Mars Global Surveyor* (Albee *et al.*, 1998) reveal a 5 km elevation difference with a corresponding dichotomy in surface roughness between the



Prelude preprint MS#4727

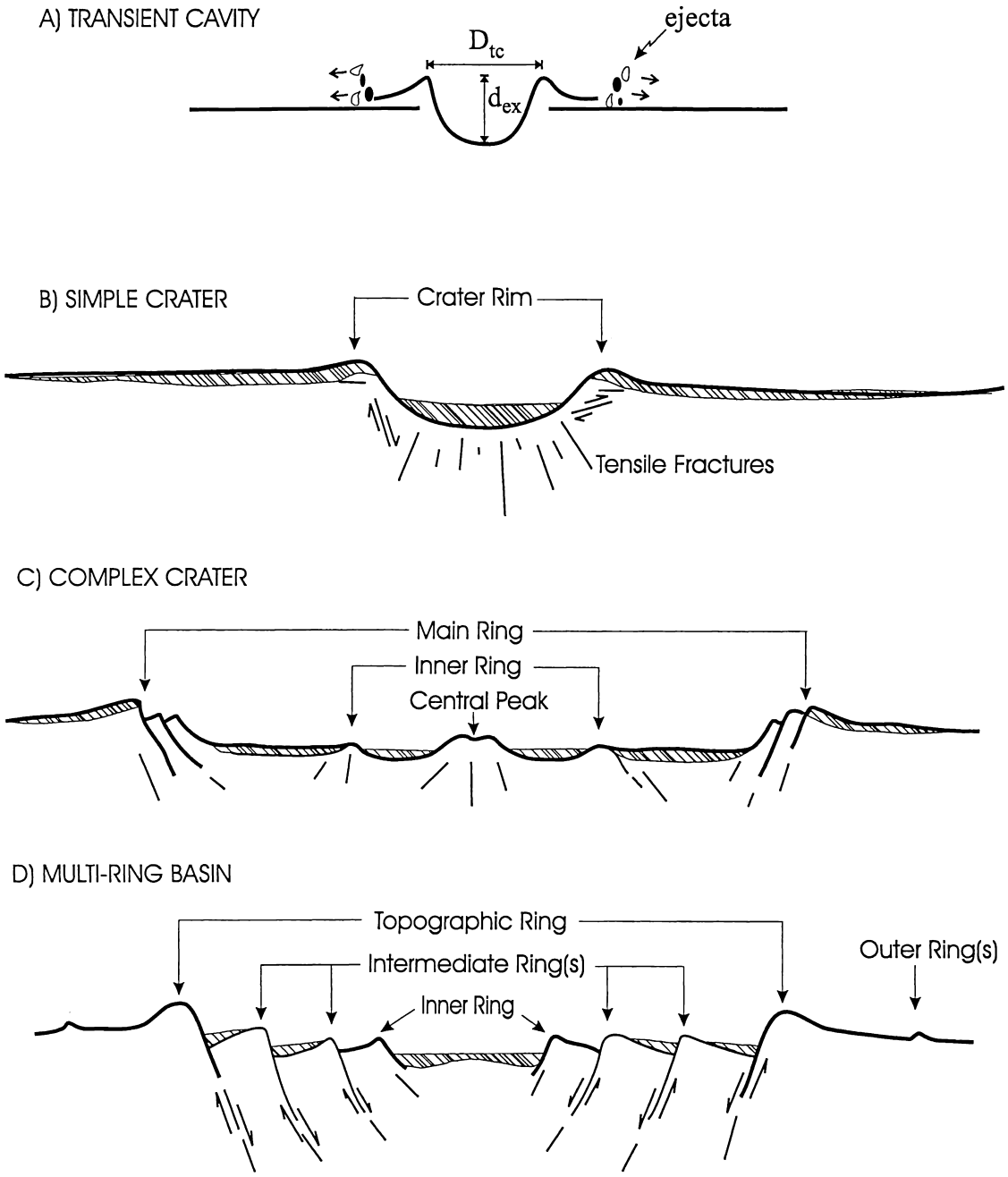


FIG. 1. Generalized crater morphologies (adapted from Wilhelms, 1987; Melosh, 1989; Spudis, 1993). The growth of the transient cavity is characterized by its diameter ($D_{tc}$) and depth ($d_{ex}$) properties. Hatching indicates possible distributions of the impact melt sheet.

northern and southern hemispheres (Aharonson *et al.*, 2001). The rougher topography in the southern hemisphere is older and heavily cratered relative to the smoother, younger, and lightly cratered topography of the northern hemisphere (Smith *et al.*, 1999) that was formed by a resurfacing event in the early development of Mars (*e.g.*, Mutch *et al.*, 1976; Carr, 1981). Studies on the internal structure of Mars from gravity and topography (*e.g.*, Kiefer *et al.*, 1996; Zuber *et al.*, 2000) also show a complementary hemispheric dichotomy in lithospheric strength and crustal thickness. The lower crustal growth rate in the northern hemisphere may be attributed to higher heat flow in early martian tectonic development (Zuber *et al.*, 2000), but the survival of large-scale topographic features in the southern hemisphere suggests that the thickness variations of the crust may have constrained topographic relaxation (Nimmo and Stevenson, 2001).

Compared to the Moon and Mars, relatively little is known about the crustal attributes of Mercury despite a limited flyby of the *Mariner 10* spacecraft (Murray *et al.*, 1974; Connerney and Ness, 1988). However, comparative planetology studies

suggest strong similarities for regolith composition and crater depth-to-diameter ratios between the Moon and Mercury (Pike, 1988). Photogeologic mapping (Spudis and Guest, 1988) also suggests that mercurian basins experienced comparable modification processes such as impact-induced uplift, isostatic relaxation, and volcanic infilling (*e.g.*, Harmon and Campbell, 1988; Pike, 1988). In addition, the mercurian multi-ring basins follow the ubiquitous planetary $\sqrt{2}D$-spacing rule for the rings of large impact basins, where $D$ is the diameter of any one of the rings (*e.g.*, Pike, 1988; Spudis, 1993).

Hence, despite the lack of gravity data for Mercury, inferences on the rheological attributes of its crust may be possible by comparing the surface roughness and transient cavity diameters or related ring attributes over its multi-ring basins to those on the Moon and Mars. As a test, we consider an improved digital elevation model (DEM) from a re-analysis of *Mariner 10* stereo image pairs (Cook and Robinson, 2000) for the Beethoven multi-ring basin of Mercury (Spudis and Guest, 1988). For new insight on the mercurian crust, the surface roughness and transient cavity diameter from the photographically estimated DEM are compared with the trends developed from combined gravity and topographic analyses of the multi-ring basins of the Moon and Mars.

In the sections that follow, we describe the application of advanced spectral correlation theory to free-air and terrain gravity data for modeling the crustal properties (*e.g.*, thickness variations, transient cavity diameters, isostatic attributes) of the multi-ring basins on the Moon and Mars. We also investigate the relationships between transient cavity attributes and the root-mean-squared topography on the Moon, Mars, and Mercury, and consider their inferences for the rheological properties of the mercurian crust.

## RING ATTRIBUTES OF IMPACT BASINS

Basin rings provide insight on the development of the transient cavity that was initiated upon impact (*e.g.*, Melosh, 1989). As summarized in Fig. 1, the rapid passage of the shock wave through the target causes the transient cavity, defined by the interface between the vapor and melted or solid components of the cavity floor, to grow by continuously ejecting material until its maximum depth ($d_{ex}$) and diameter ($D_{tc}$) are attained (Melosh, 1989). The cratering process starts with the growing transient cavity (Fig. 1a) that collapses into either a simple crater (Fig. 1b), a complex crater (Fig. 1c), or a multi-ring basin (Fig. 1d). The final morphology depends on a range of factors including the gravity field of the planet, the physical properties of the substrate or target conditions and the atmosphere, as well as the projectile's size, speed, and trajectory (*e.g.*, Wilhelms, 1987; Melosh, 1989).

Identifying the transient cavity diameter ($D_{tc}$) provides insight on various impact parameters including the mechanism for basin formation, crustal volume displacement, sample provenance, origin of mascons (*e.g.*, Spudis, 1993), and crustal viscosity (*e.g.*, Melosh, 1982). Photogeologic interpretations have identified the ubiquitous $\sqrt{2}D$-spacing rule for the rings of the large impact basins on the planets (*e.g.*, Wilhelms, 1987; Melosh, 1989). A common estimate of $D_{tc}$ is provided by the diameter of the innermost ring (*e.g.*, Floran and Dence, 1976; Spudis *et al.*, 1984; Wilhelms, 1987; Melosh, 1989). However, the innermost ring location in photographs can be obscured by ejecta, lava flooding, and other blanketing effects from basin-forming processes (*e.g.*, Wilhelms, 1987; Melosh, 1989). Accordingly, gravity-based methods that are largely insensitive to these masking effects have also been used for estimating transient cavity diameters in the crust (Wieczorek and Phillips, 1999; Potts and von Frese, 2001b).

### Basin Ring Diameters Estimated from Gravity

Central basin and ring formation processes clearly produce mass variations that will be reflected in the topographic and gravity data of the impact basin. Wieczorek and Phillips (1999) related a dual-layered crustal model of the Moon to Bouguer anomalies in an attempt to restore the lunar Moho to its pre-impact position beneath the basins. The geometric crustal reconstruction produced roughly parabolic crustal depressions from which transient cavity depths and diameters were estimated.

In another approach, transient cavity diameters were estimated from the spectral correlation of free-air and computed terrain gravity effects at satellite altitudes for the Moon (Potts and von Frese, 2001a,b) and Mars (Potts and von Frese, 2001c). This method produces a more comprehensive account of the ring structure for the impact basins than can be obtained by geometric crustal reconstruction. However, as discussed in the next section the two methods provide remarkably similar estimates for the lunar transient cavity diameters.

The principal features of using the spectral correlation of the gravity effects to model the crust of multi-ring basins on the Moon and Mars are demonstrated in Fig. 2. For the Moon, the free-air anomaly components from the Lunar Prospector LP75G gravity model (Konopliv *et al.*, 1998) were spectrally correlated at 100 km altitude with the gravity effects of the Clementine GLTM-2 terrain model (Smith *et al.*, 1997). For Mars, we compared, also at 100 km altitude, gravity data from the *Mars Global Surveyor* (Lemoine *et al.*, 2001) with the gravity effects of the topography mapped by the *Mars Orbiter* laser altimeter (Smith *et al.*, 1999). In both cases, the gravity effects of the topography were computed in spherical coordinates at satellite altitudes using Gauss–Legendre quadrature integration (von Frese *et al.*, 1981, 1997b) and 2.8 g/cm$^3$ terrain density.

The left and right panels in Fig. 2 show the results across representative lunar and martian multi-ring basins, respectively. Figure 2a gives the free-air gravity anomalies at 100 km altitude along with their related terrain-correlated and terrain-decorrelated components. These components were obtained

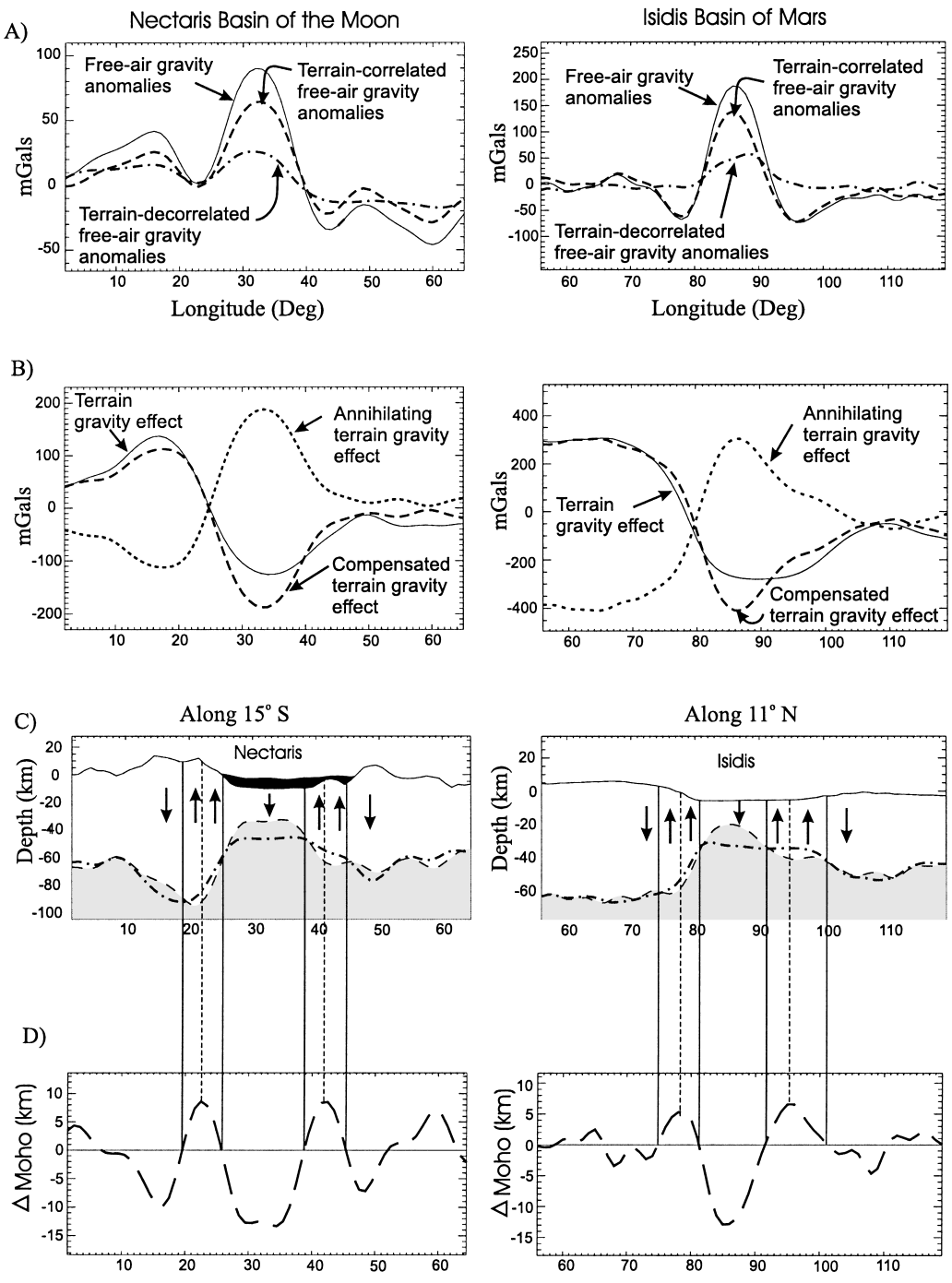


FIG. 2. Spectral correlation modeling of the free-air and terrain gravity effects for typical multi-ring basins on the Moon (left panel) and Mars (right panel). The shaded portion at the top of the lunar Nectaris Basin represents basin mare fill estimated from the terrain-decorrelated gravity anomalies (Potts and von Frese, 2001a). The surface relief and fill are exaggerated by a factor of 2 in (c).

using correlation filters based on the correlation spectrum (von Frese *et al.*, 1997a) between the free-air anomalies (Fig. 2a) and the computed terrain gravity effects in Fig. 2b. The spectral correlation filters were designed so that the terrain-decorrelated anomalies (Fig. 2a) and compensated terrain effects (Fig. 2b) have effectively zero correlation, and hence may be independently analyzed for the properties of the subsurface.

For this application, we assumed the crust was primarily compensated by its thickness variations with the terrain-correlated free-air anomalies reflecting mostly the effects of uncompensated terrain. Accordingly, the terrain-decorrelated anomalies and compensated terrain effects were obtained by subtracting the terrain-correlated components from the free-air and terrain gravity effects, respectively.

The lack of compensated terrain effects in the free-air anomalies can be explained by annihilating signals that may be analyzed for Moho variations in the context of an appropriate crustal compensation model. Reversing the polarities of the compensated terrain effects yielded the annihilating signals shown in Fig. 2b. Assuming the crust was compensated primarily by its thickness variations, the Moho estimates (dashed curve) in Fig. 2c were then obtained by spherical coordinate inversions of the annihilating signals using Gauss–Legendre quadrature integration. In these inversions, density contrasts of 0.5 and 0.6 g/cm$^3$ for the mantle relative to the crust were assumed for the Moon and Mars, respectively.

This methodology was developed and validated in crustal studies of the Antarctic (von Frese *et al.*, 1999) and East Asia (Tan and von Frese, 1997; Tan, 1998; von Frese *et al.*, 1998), where the gravity estimated Moho depths were found to be well within 10% of the depths inferred by large offset seismic studies. The methodology was also used for crustal analyses of the Moon (Potts, 2000) and its Mare Orientale Basin (von Frese *et al.*, 1997b, 1998), Greenland (Roman, 1999), and Venus (Leftwich *et al.*, 1999).

In Fig. 2c, we also estimated the equilibrium Moho (dot-dashed curve), which completely nullifies the terrain gravity effect, from the inversion of the terrain-correlated free-air anomalies that we take to reflect the effects of mostly uncompensated crust. The crust is presumably attempting to achieve complete isostatic equilibrium and a zero mean free-air gravity anomaly. Hence, where the Moho is above or below the equilibrium Moho, the mantle is at superisostatic or subisostatic levels, respectively, and the crust may be under pressure to sink or rise.

The differences (ΔMoho) between the Moho and equilibrium Moho are shown in Fig. 2d. These differences are very strongly correlated with the positions of the basin rings that are marked by the vertical lines connecting Fig. 2c and Fig. 2d. Specifically, starting from the basin center, the innermost ring is located at the first zero cross-overs of the differences (solid vertical lines), with the second ring occurring at the next flanking maximum/minimum difference (dashed lines), the third ring at the next zero cross-overs, and so forth. The arrows in the crustal cross-sections of Fig. 2c indicate the relative motions that the crust must undergo between the rings to nullify the terrain-correlated free-air anomalies.

For the Moon, nearly every photogeologically identified basin ring was found to be located at either a zero or maximum/minimum Moho difference, although not all of these differences have been attributed to basin rings by photogeologic analysis (Potts, 2000; Potts and von Frese, 2001b). The very strong correlation between the ring diameters inferred from photogeologic studies (PG) and the gravity-derived Moho differences (ΔMoho) is indicated in Fig. 3. For this comparison, the photogeologic estimates from Solomon and Head (1980), Wilhelms (1987), and Spudis (1993) were used that included ring diameter estimates based on the $\sqrt{2}D$-spacing rule (Spudis, 1993). The remarkable correlation of 0.99 for the lunar basins in Fig. 3 suggests that effective estimates on the size, location, and number of basin rings may be obtained from the terrain-correlated free-air gravity anomalies.

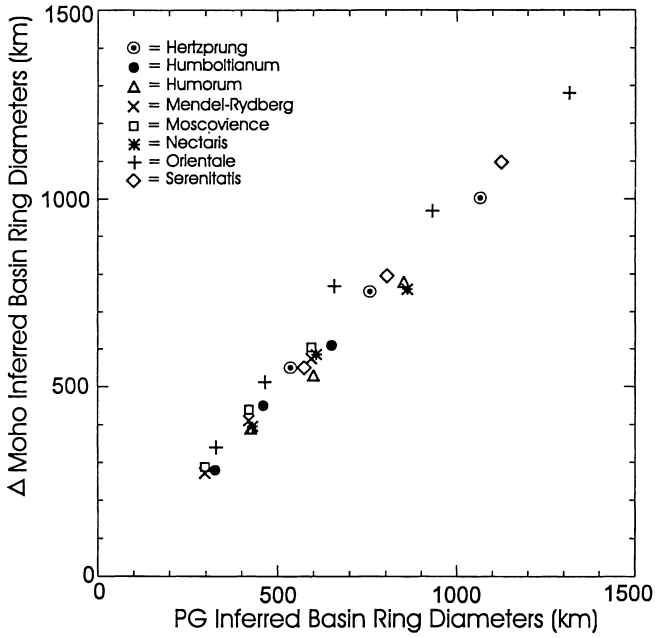


FIG. 3. Comparison of basin ring diameters inferred from photogeological (PG) estimates (Solomon and Head, 1980; Wilhems, 1987; Spudis, 1993) and the Moho adjustments (ΔMoho) that annihilate the terrain-correlated free-air gravity anomalies of major lunar basins.

## Estimating Transient Cavity Diameters

The dimensions of the transient cavity provide insight on the mechanical properties of the crust (*e.g.*, Melosh, 1982; Spudis, 1993). Transient cavity diameters ($D_{tc}$) have been estimated from photogeologic interpretations of the topographic rim diameters (Wilhelms, 1987), inner ring diameters (*e.g.*, Floran and Dence, 1976), the distribution of shock metamorphism in bedrock (*e.g.*, Murtaugh, 1972), and pre-impact landforms (Spudis *et al.*, 1984). In general, the diameter of the inner ring may provide the most common estimate of $D_{tc}$ (*e.g.*, Floran and Dence, 1976; Spudis *et al.*, 1984; Melosh, 1989), but the location of the inner ring can be obscured by the masking effects from basin-forming processes (*e.g.*, Wilhelms, 1987; Melosh, 1989).

Alternate estimates of $D_{tc}$ are clearly possible using the innermost ring diameters derived from the terrain-correlated free-air anomalies as described in the previous section. Geometric crustal reconstruction provides another gravity-based method for effectively estimating transient cavity diameters (Wieczorek and Phillips, 1999). Figure 4 compares the $D_{tc}$ estimates from the two gravity-based approaches for 10 nearside lunar basins studied by Wieczorek and Phillips

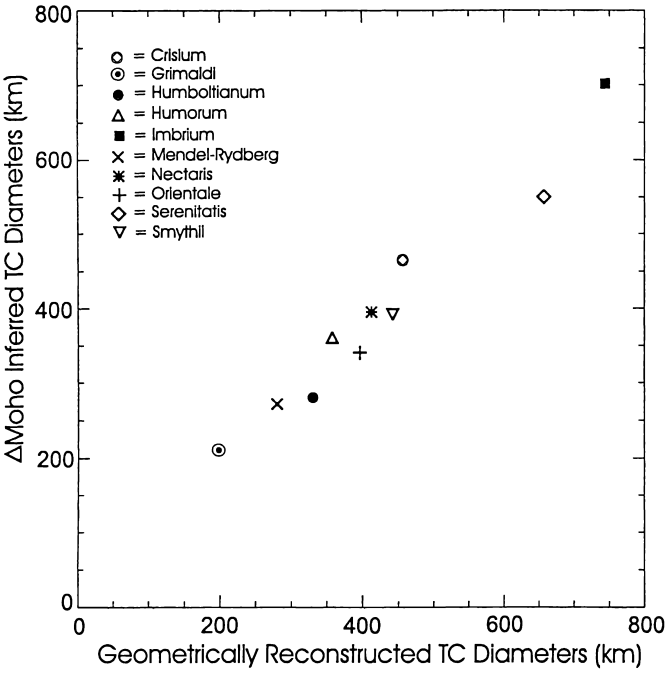


FIG. 4. Comparison of transient cavity (TC) diameters determined by geometric crustal reconstruction (Wieczorek and Phillips, 1999) and the Moho adjustments (ΔMoho).

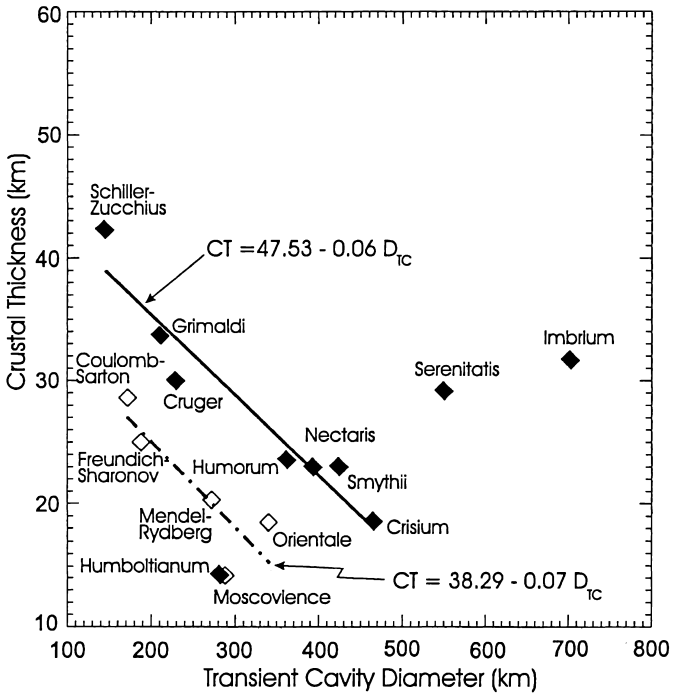


FIG. 5. Crustal thickness (CT) and transient cavity diameter ($D_{tc}$) estimates for lunar nearside (solid diamonds) and farside (open diamonds) multi-ring basins with overcompensating or superisostatic mantle plugs.

(1999). The strongly linear agreement with a 0.98 coefficient of correlation suggests that the two methods yield remarkably consistent $D_{tc}$ estimates.

## TRANSIENT CAVITY DIAMETER AND CRUSTAL THINNING

The excavation of large quantities of crustal material presumably facilitated the uplift of the Moho beneath multi-ring basins (Melosh, 1989). However, crustal thinning by crustal unloading and mantle uplift is related to basin formation, whereas ring development is related to the basin modification phase (Melosh, 1989; Spudis, 1993). Accordingly, crustal thickness may be correlated more with the transient cavity diameter that developed during the basin excavation process than with the size of the basin's main rim (*e.g.*, Neumann *et al.*, 1996).

Insights on the $D_{tc}$ and its possible extensions by correlated parameters such as crustal thickness can facilitate assessing the mechanical properties of the lithosphere. For example, the positive trend between crustal viscosity and $D_{tc}$ (Melosh, 1989) predicts larger $D_{tc}$ as viscosity presumably increased with time following the bombardment period when high near-surface temperatures associated with impact heating were prevalent (Solomon *et al.*, 1982). Hence, the relationship between crustal thickness and $D_{tc}$ for basins involving mass distributions with contrasting isostatic properties may be especially useful for investigating the diverse lithospheric mechanical properties of the Moon and Mars.

### Lunar Crustal Attributes

From the spectral correlation of lunar free-air and terrain gravity effects between ±64° latitudes, we estimated crustal thickness and $D_{tc}$ for the multi-ring basins. Figure 5 shows scatter plots of these results for both nearside (solid symbols) and farside (open symbols) basins with superisostatic mantle plugs.

The solid line in Fig. 5 along with its equation in kilometers plots the inverse least-squares trend for the superisostatic basins of the nearside. Outliers to this equation may include the Humboltianum, Imbrium, and Serenitatis Basins. The crustal properties established for Humboltianum may be problematic in this analysis because the basin is located at high latitudes where topographic accuracies are poor (*e.g.*, Neumann *et al.*, 1996; Smith *et al.*, 1997). The crustal properties for Serenitatis and Imbrium, on the other hand, are probably atypical of the nearside crust. These basins formed in largely resurfaced Procellarum KREEP terrane whose mafic petrogenesis may relate to the early differentiation of the Moon (Joliff *et al.*, 2000; Haskin, 1998; Korotev, 2000).

The inverse least-squares trend for farside basins with superisostatic mantle plugs is plotted by the dot-dashed line in Fig. 5 along with its equation in kilometers. As discussed in a later section ("Discussion"), the offset in these two trends tends to support the dichotomy in lithospheric properties between the lunar nearside and farside.

The results for the subisostatic multi-ring basins that are mostly confined to the lunar farside revealed little or no apparent linear association between crustal thickness and $D_{tc}$ (Potts and von Frese, 2001b) and hence were not included in Fig. 5. However, the results are consistent with the existence of a more viscous farside lithosphere during bombardment time wherein mantle plugs could develop only to subisostatic levels and the formation of basin rings was limited by a thicker and stiffer farside crust (Potts and von Frese, 2001b).

### Martian Crustal Attributes

Crustal thickness and $D_{tc}$ estimates for the martian multi-ring basins were obtained from the spectral correlation of free-air and terrain gravity effects. The results are shown in Fig. 6, where the least-squares inverse trend is plotted by the dashed line along with its equation in kilometers.

The effects for the superisostatic basins (solid symbols) dominate the inverse association between crustal thicknesses and transient cavity diameters. An apparent outlier here is the Daedalia Basin with crust that may have experienced volcano-tectonic modification (Spudis, 1993), because it underlies the Noctis Labyrinthus, which is the center of uplift for the massive Tharsis Bulge. This inverse trend is also reflected by the results from the basins that appear to be underlain by subisostatic mantle plugs (open symbols). These include the ancient Al Qahira Basin of the Noachian period (Tanaka *et al.*, 1992; Spudis, 1993) and the presumably similar age Cassini Basin (Acuna *et al.*, 1999).

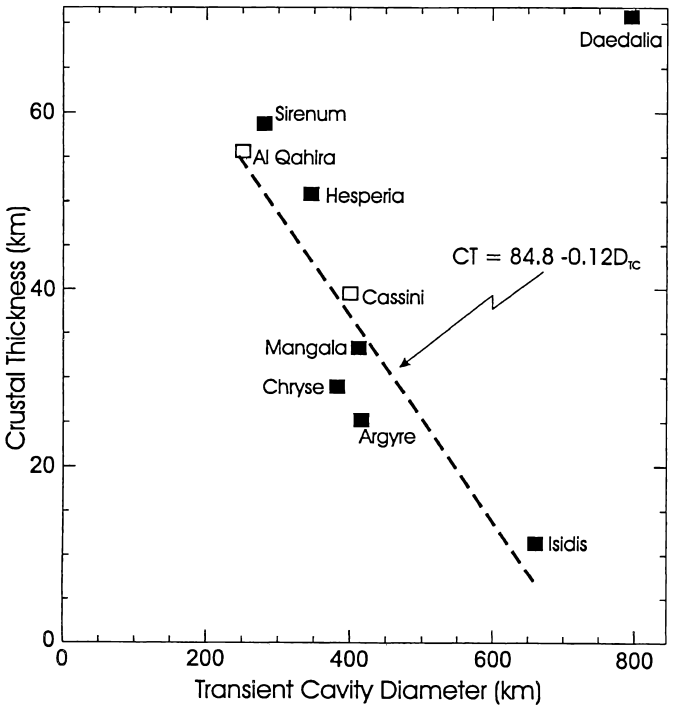


FIG. 6. Crustal thickness (CT) *vs.* transient cavity diameter ($D_{tc}$) estimates for martian basins with overcompensating (solid squares) and undercompensating or subisostatic (open squares) mantle plugs.

## MORPHOMETRICS OF THE IMPACT BASINS

Crater morphology also affords insights on the mechanical attributes of planetary lithospheres (*e.g.*, Melosh, 1982; Galdikas, 1999). For example, the dichotomy in mechanical properties between the lunar nearside and farside crust was noted from studies on surface profiles over the basins (*e.g.*, Solomon *et al.*, 1982; Williams and Zuber, 1998).

For this analysis, we evaluated the relationships between transient cavity diameters and related crater morphologies for the multi-ring basins of the Moon, Mars and Mercury. Specifically, we compared $D_{tc}$ against crater roughness ($R_q$) given by the root-mean-square topography over 64 × 64° patches centered on the multi-ring basins. For Mercury, only a preliminary DEM over the Beethoven Basin from the *Mariner 10* flyby (Cook and Robinson, 2000) was available for analysis. However, as a typical mercurian multi-ring basin (Spudis and Guest, 1988), Beethoven's topographic and ring attributes will be useful in assessing the characteristic crustal properties for Mercury.

### Surface Roughness and Transient Cavity Diameter Comparisons

Scatter plots of $R_q$ *vs.* $D_{tc}$ are given in Fig. 7. Figure 7a shows the results for lunar nearside basins that are dominated by mascons related predominantly to overcompensating or superisostatic mantle plugs. The dashed line through these results provides a least-squares estimate in kilometers of $R_q$ in terms of $D_{tc}$. This equation is not appreciably affected by deleting the results from Humboltiaum, Serenitatis and Imbrium that were considered outlier basins in the analysis of Fig. 5. This trend also correlates directly with the relative ages of the nearside basins (Wilhelms, 1987).

Figure 7b gives the results for the lunar farside that includes both superisostatic (solid symbols) and subisostatic (open symbols) basins. The results are more scattered than they were for the nearside. However, the least-squares equation for the positive linear trend (dashed line) defined by the data has the same slope, but larger intercept values in kilometers.

Figure 7c demonstrates the results for Mars that also includes both superisostatic (solid symbols) and subisostatic (open symbols) basins. Again, the least-squares trend (dashed line) is positive with a slightly higher slope and somewhat lower intercept than the trend for the lunar nearside basins. We excluded the Daedalia Basin in our derivation of the equation in Fig. 7c, because its ballistic morphology may have been strongly affected by the relief and volcano-tectonic processes of the great Tharsis Buldge (Spudis, 1993).

Figure 7d compares the results for the Beethoven Basin of Mercury with the least-squares trends obtained in the other three panels for the Moon and Mars. The values for $R_q$ and

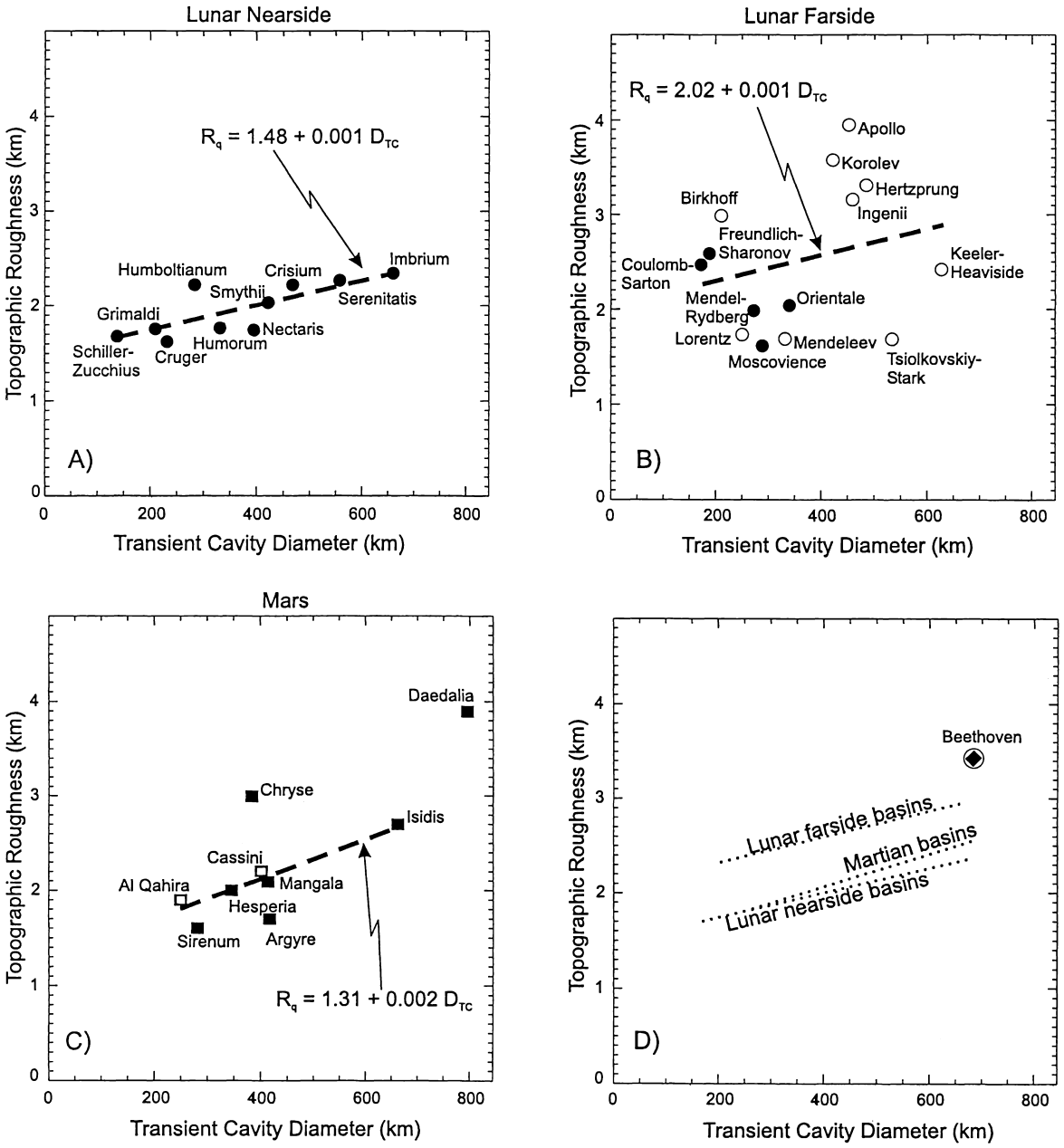


FIG. 7. Comparison of surface roughness ($R_q$) and transient cavity diameter ($D_{tc}$) estimates for multi-ring basins on the lunar nearside (a) and farside (b), and Mars (c) and Mercury (d). In (b) and (c), solid and open symbols indicate superisostatic and subisostatic basins, respectively.

$D_{tc}$ of the Beethoven Basin are based on imagery that was taken at high Sun angle where only a single ring is clearly discernible (Spudis and Guest, 1988). However, additional DEMs are being processed from the *Mariner 10* stereo imagery for other mercurian basins (Cook, 2001, pers. comm.) that may be soon available to augment and test these results.

## DISCUSSION

Crustal modeling of lunar free-air and terrain gravity correlations suggests that superisostatic mantle plugs may predominantly underly multi-ring basins of the nearside, while subisostatic mantle plugs mostly underly the farside basins. In general, these results are consistent with a nearside crust that was thinner, hotter and less rigid than the farside crust during bombardment time (Solomon *et al.*, 1982).

For the superisostatic basins of the lunar nearside and farside, the $D_{tc}$ and crustal thicknesses estimates (Fig. 5) reveal distinct linear trends with similar slopes, but quite different intercepts. This offset between the two inverse trends suggests that the farside basins may have developed in a much stronger lithosphere than the nearside basins. In particular, because of

its greater strength, the thickness of the farside crust wherein superisostatic mantle plugs were produced was probably no greater than ~75% of the thickness of the nearside crust in which these plugs were emplaced.

In general, our modeling found that the production of superisostatic mantle plugs was apparently limited to crustal thicknesses of perhaps 30 km, whereas in thicker crust the mantle plugs appear to have developed only to subisostatic levels (Potts and von Frese, 2001a). Moreover, the transient cavity diameters for the superisostatic basins were generally smaller than those of the subisostatic basins that are predominantly located on the farside. Hence, in view of the direct proportionality of viscosity with $D_{tc}$ (Head, 1982; Melosh, 1982; Alexopoulos and McKinnon, 1994), our results provide additional support for the dichotomized viscosity between the nearside and farside during bombardment time.

The negative trend in Fig. 5 for the lunar nearside also correlates inversely with the relative ages of the superisostatic basins (Wilhelms, 1987). The correlation may reflect the development of thicker crust for the older basins due to greater subsidence of the uplifted Moho in a warmer lithosphere compared to more limited subsidence for the younger basins in a colder, more viscous lithosphere.

For Mars, a clearly negative linear relationship between the $D_{tc}$ and crustal thickness estimates was found (Fig. 6). This trend also appears to be inversely correlated with basin ages from a broad time-stratigraphic classification that includes the Noachian (oldest), Hesperian, and Amazonian (youngest) periods (Cattermole, 1992). Although this scheme of relative basin ages is poorly constrained for lack of radiometric dating of the martian rocks, its use with our results is consistent with crustal rigidity that increased over time.

For example, the older Noachian basins, Al Qahira and Sirenum, and the Hesperian Basin, Hesperia, were formed in the thicker crust of the southern hemisphere relative to the presumably younger Amazonian Basin, Isidis, that formed in the thinner crust of the northern hemisphere which suffered considerable resurfacing and heat loss (Zuber *et al.*, 2000). However, analysis of the magnetic observations from the *Mars Global Surveyor* suggests that remnants of the original crust may also exist beneath the volcanic cover (Hood and Zakharian, 2001). Our terrain-decorrelated gravity anomalies also support this notion. These data reveal ringed free-air anomalies over the northern hemisphere that may target buried basins which can be modeled by crustal effects like those shown for the Isidis Basin in Fig. 2. In general, the satellite free-air anomalies are key indicators of uncompensated mass components for both buried and topographically visible impact basins.

Our spectral correlation studies of the free-air and terrain gravity effects for the multi-ring basins of the Moon and Mars suggest that the $D_{tc}$ and topography are indicative of the rheological properties of the crust. For Mercury where gravity data are lacking, alternate estimates of these parameters from photometric studies must be used. To test the viability of this approach, we developed relationships between $R_q$ and $D_{tc}$ in Fig. 7a–c for the lunar and martian basins.

The direct correspondence of lunar $D_{tc}$ with $R_q$ values also suggests the dichotomized rheological properties of crust at the time of bombardment. For the nearside (Fig. 7a), the results are proportional to the relative ages of the basins, suggesting increased crustal rigidity with time. The positive offset of the linear trend for the farside basins (Fig. 7b) relative to the trend of the nearside basins is also consistent with basin impacts on a comparatively stronger farside lithosphere.

For Mars, $R_q$ is also positively correlated with $D_{tc}$ (Fig. 7c). The slope is consistent with the rough relative ages of the basins (Cattermole, 1992). However, the intercept is better matched with the trend for the lunar nearside basins than that of the farside basins. Hence, the highland crust appears to have responded rheologically to bolide impacts more like the crust of the lunar nearside than the farside during bombardment time.

For Mercury, we have at present only the photometric results from the Beethoven Basin to compare against the lunar and martian trends (Fig. 7d). The comparison, however, suggests that the mechanical attributes of Mercury's lithosphere were most comparable to those of the lunar farside during bombardment time. However, relative to the Moon, the rigid mercurian crust was much hotter and a thicker lithosphere was developed on Mercury by the end of the heavy bombardment period (Melosh and McKinnon, 1988). Our result supports an early hot, but high viscosity mercurian surface that is consistent with a "dry" crust (*e.g.*, Schultz, 1988; Barlow *et al.*, 1999; Mackwell *et al.*, 1998) for a volatile-poor planet (*e.g.*, Goettel, 1988).

Additional testing of our inferences on the poorly understood mercurian crust will occur as more photometric DEMs of the basins become available (Cook, 2001, pers. comm.). However, the number of photometrically identifiable multi-ring basins appears to have been limited by the viscous relaxation of the topography (Melosh and McKinnon, 1988). The crust of Mercury was exposed to temperatures up to roughly 200 K hotter than what the lunar crust experienced, so crustal viscosities may have been reduced by up to 2 orders of magnitude relative to those of the lunar crust if similar compositional and thermal properties are assumed (Melosh and McKinnon, 1988). Hence, significant new insight on the poorly understood crustal properties of Mercury are anticipated from the gravity and topography data that will be obtained by the proposed MESSENGER mission.

## CONCLUSION

We analyzed free-air and topographic gravity correlations for crustal mass variations of the Moon and Mars to constrain the $D_{tc}$ and crustal thickness estimates beneath the multi-ringed impact basins. For the Moon, crustal rigidity appears to hold impact-induced mass disruptions at predominantly superisostatic and subisostatic levels for the nearside and

farside, respectively. A weaker nearside lithosphere facilitated the development of a thinner crust while the farside yielded a more brittle response to impacts due to its higher viscosity.

For Mars, our results suggest a linear decrease of crustal thickness with time. Older basins developed thicker crust in the southern hemisphere presumably due to enhanced thermal insulation, while younger basins developed thinner crust in the northern hemisphere of high heat loss.

The photometric correlation of $R_q$ with $D_{tc}$ estimates can provide comparable insights on the crustal properties for regions such as Mercury that lack gravity data. For example, the trend in $R_q$ for the lunar nearside basins is depressed by ~0.5 km relative to the farside basins. This offset is consistent with the development on the nearside of relatively subdued basin morphology in a lithosphere with a higher thermal gradient from a greater abundance of radiogenic elements. More rugged topography developed on the lunar farside where a lower thermal gradient resulted in a more brittle response to bolide impacts. The trend for Mars correlates most strongly with the trend of the lunar nearside, whereas the results for the Beethoven Basin reflect a relatively rigid crust for Mercury with rheological attributes that were more like those of the lunar farside crust.

*Acknowledgments*–We thank J. Grier and two other anonymous reviewers for their helpful comments. A. S. Konopliv and F. Lemoine kindly provided the respective lunar (LP75G) and martian (GMM2B) gravity fields through the Geoscience Data Node of the Planetary Data System. We also thank A. C. Cook for making available photometric elevation data for Mercury's Beethoven Basin for this study. Grants from NASA Goddard Space Flight Center (PO S-97647-Z) and the Laboratory for Space Geodesy and Remote Sensing Research at The Ohio State University supported elements of this research.

*Editorial handling*: W. K. Hartmann

## REFERENCES

ACUNA M. H. *ET AL.* (1999) Global distribution of crustal magnetization discovered by the Mars Global Surveyor MAG/ER experiment. *Science* **284**, 790–793.

AHARONSON O., ZUBER M. T. AND ROTHMAN D. (2001) Statistics of Mars' topography from the Mars orbiter laser altimeter: Slopes, correlations, and physical models. *J. Geophys. Res.* **106**, 23 723–23 735.

ALBEE A. L., PALLUCONI F. D. AND ARVIDSON R. E. (1998) Mars Global Surveyor mission: Overview and status. *Science* **279**, 1671–1672.

ALEXOPOULOS J. S. AND MCKINNON W. B. (1994) Large impact craters and basins on Venus, with implications for ring mechanics on the terrestrial planets. *Geol. Soc. Am. Spec. Paper* **293**, 29–50.

BARLOW N., ALLEN R. AND VILAS F. (1999) Mercurian impact craters: Implications for polar ground ice. *Icarus* **141**, 194–200.

BINDER A. (1998) Lunar Prospector: Overview. *Science* **281**, 1475–1476.

CARR M. H. (1981) *The Surface of Mars.* Yale Univ. Press, New Haven, Connecticut, USA. 232 pp.

CATTERMOLE P. (1992) *Mars: The Story of the Red Planet.* Chapman and Hall, New York, New York, USA. 224 pp.

CONNERNEY J. E. P. AND NESS N. F. (1988) Mercury's magnetic field and interior. In *Mercury* (eds. F. Vilas, C. R. Chapman and M. S. Matthews), pp. 494–513. Univ. Arizona Press, Tucson, Arizona, USA.

COOK A. AND ROBINSON M. S. (2000) Mariner 10 stereo image coverage of Mercury. *J. Geophys. Res.* **105**, 9429–9443.

FLORAN R. J. AND DENCE M. R. (1976) Morphology of the Manicouagan ring-structure, Qeubec, and some comparisons with lunar basins and craters. *Proc. Lunar Sci. Conf.* **7th**, 2845–2865.

GALDIKAS A. (1999) Surface topography development and ion mixing in the study of depth profiling of multi-layered structures. *Vacuum* **55**, 51–58.

GOETTEL K. (1988) Present bounds on the bulk composition of Mercury: Implications for planetary formation processes. In *Mercury* (eds. F. Vilas, C. R. Chapman and M. S. Matthews), pp. 613–621. Univ. Arizona Press, Tucson, Arizona, USA.

HARMON J. AND CAMPBELL D. (1988) Radar observation of Mercury. In *Mercury* (eds. F. Vilas, C. R. Chapman and M. S. Matthews), pp. 101–117. Univ. Arizona Press, Tucson, Arizona, USA.

HASKIN L. A. (1998) The Imbrium impact event and the thorium distribution at the lunar highlands surface. *J. Geophys. Res.* **103**, 1679–1690.

HEAD J. W. (1982) Lava flooding of ancient planetary crusts: Geometry, thickness, and volumes of flooded lunar impact basins. *Moon and Planets* **26**, 61–88.

HOOD L. L. AND ZAKHARIAN A. (2001) Mapping and modeling of magnetic anomalies in the northern polar regions of Mars. *J. Geophys. Res.* **106**, 14 601–14 619.

JOLIFF B. L., GILLIS J. J., HASKIN L. A., KOROTEV R. L. AND WIECZOREK M. A. (2000) Major lunar crustal terranes: Surface expressions and crust-mantle origins. *J. Geophys. Res.* **105**, 4217–4235.

KIEFER W. S., BILLS B. G. AND NEREM R. S. (1996) An inversion of gravity and topography for mantle and crustal structure on Mars. *J. Geophys. Res.* **101**, 9239–9252.

KONOPLIV A. S., BINDER A. B., HOOD L. L., KUCINSKAS A. B., SJORGEN W. L. AND WILLIAMS J. G. (1998) Improved gravity field of the Moon from Lunar Prospector. *Science* **281**, 1476–1480.

KOROTEV R. (2000) The great lunar hot spot and the composition and origin of the Apollo mafic ("LFKM") impact-melt breccias. *J. Geophys. Res.* **105**, 4317–4346.

LEFTWICH T., VON FRESE R., KIM H., POTTS L. V., ROMAN D. AND TAN L. (1999) Crustal analysis of Venus from Magellan satellite observations at Atalanta Planitia, Beta Regio and Thetis Regio. *J. Geophys. Res.* **104**, 8441 – 8462.

LEMOINE F. G., SMITH D. E., ROWLANDS D. D., ZUBER M. T., NEUMANN G. A., CHINN D. S. AND PAVLIS D. E. (2001) An improved solution of the gravity field of Mars (GMM-2B) from Mars Global Surveyor. *J. Geophys. Res.* **106**, 23 359–23 376.

LUCEY P. G., SPUDIS P. D., ZUBER M., SMITH D. AND MALARET E. (1994) Topographic-compositional units on the Moon and early evolution of the lunar crust. *Science* **266**, 1855–1858.

MACKWELL S., ZIMMERMAN M. AND KOHLSTEDT D. (1998) High-temperature deformation of dry diabase with application to tectonics on Venus. *J. Geophys. Res.* **103**, 975–984.

MELOSH H. J. (1982) A schematic model of crater modification by gravity. *J. Geophys. Res.* **87**, 371–380.

MELOSH H. J. (1989) *Impact Cratering: A Geologic Process.* Oxford Univ. Press, New York, New York, USA. 245 pp.

MELOSH H. J. AND MCKINNON W. B. (1988) Tectonics on Mercury. In *Mercury* (eds. F. Vilas, C. R. Chapman and M. S. Matthews), pp. 374–428. Univ. Arizona Press, Tucson, Arizona, USA.

MURRAY B. *ET AL.* (1974) Mercury's Surface: Preliminary description and interpretation from Mariner 10 pictures. *Science* **185**, 169–179.

MURTAUGH J. G. (1972) Shock metamorphism in the Manicouagan crypto-explosion structure. *Proc. 24th Geol. Congr.* **Sect. 15**, 133–139.

MUTCH T. A., ARVIDSON R. E., HEAD J. W., JONES K. L. AND SAUNDERS R. S. (1976) *The Geology of Mars*. Princeton Univ. Press, Princeton, New Jersey, USA. 400 pp.

NEUMANN G. A., ZUBER M. T., SMITH D. E. AND LEMOINE F. G. (1996) The lunar crust: Global structure and signature of major basins. *J. Geophys. Res.* **101**, 16 841–16 843.

NIMMO F. AND STEVENSON D. J. (2001) Estimation of martian crustal thickness from viscous relaxation of topography. *J. Geophys. Res.* **106**, 5085–5098.

NOZETTE S., SMITH D. E. AND LEMOINE F. G. (1994) The Clementine mission to the Moon: Scientific overview. *Science* **266**, 1835–1838.

PIKE R. J. (1988) Geomorphology of impact craters on Mercury. In *Mercury* (eds. F. Vilas, C. R. Chapman and M. S. Matthews), pp. 165–273. Univ. Arizona Press, Tucson, Arizona, USA.

POTTS L. V. (2000) Satellite geophysical investigation of the Moon. Ph.D. thesis, The Ohio State University, Columbus, Ohio, USA. 296 pp.

POTTS L. V. AND VON FRESE R. R. B. (2001a) Lunar basin ring and transient cavity attributes from spectrally correlated free-air and terrain gravity data (abstract). *Eos Trans. AGU* **82(20)**, P22A-04.

POTTS L. V. AND VON FRESE R. R. B. (2001b) Lunar subcrustal mass variations from spectrally correlated free-air and terrain gravity effects (abstract). *Eos Trans. AGU* **82(20)**, P41B-05.

POTTS L. V. AND VON FRESE R. R. B. (2001c) Martian mass differentiation from spectrally correlated free-air and topographic gravity data (abstract). *Eos Trans. AGU* **82(20)**, P32A-12.

ROMAN D. R. (1999) An integrated geophysical investigation of Greenland's tectonic history. Ph.D. thesis, The Ohio State University, Columbus, Ohio, USA. 270 pp.

SCHULTZ P. (1988) Cratering on Mercury: A relook. In *Mercury* (eds. F. Vilas, C. R. Chapman and M. S. Matthews), pp. 118–164. Univ. Arizona Press, Tucson, Arizona, USA.

SMITH D. E., ZUBER M. T., NEUMANN G. A. AND LEMOINE F. G. (1997) Topography of the Moon from the Clementine Lidar. *J. Geophys. Res.* **102**, 1591–1611.

SMITH D. E. *ET AL.* (1999) Global topography of Mars and implications for surface evolution. *Science* **284**, 1495–1503.

SOLOMON S. C. AND HEAD J. W. (1980) Lunar mascon basins: Lava filling, tectonics and evolution of the lithosphere. *Rev. Geophys. Space Phys.* **18**, 107–141.

SOLOMON S. C., COMER R. P. AND HEAD J. W. (1982) The evolution of impact basins: Viscous relaxation of topographic relief. *J. Geophys. Res.* **87**, 3975–4000.

SPUDIS P. (1993) *The Geology of Multi-Ring Impact Basins: The Moon and Other Planets*. Cambridge Univ. Press, New York, New York, USA. 263 pp.

SPUDIS P. D. AND GUEST J. E. (1988) Stratigraphy and geologic history of Mercury. In *Mercury* (eds. F. Vilas, C. R. Chapman and M. S. Matthews), pp. 118–164. Univ. Arizona Press, Tucson, Arizona, USA.

SPUDIS P. D., HAWKE B. R. AND LUCEY P. (1984) Composition of Orientale basin deposits and implications for the lunar basin-forming process. *J. Geophys. Res.* **89 (Suppl.)**, C197–C210.

STEVENSON D. J. (1980) Lunar asymmetry and palaeomagnetism. *Nature* **287**, 520–521.

TAN L. (1998) Lithospheric analysis of satellite geopotential anomalies of East Asia. Ph.D. thesis, The Ohio State University, Columbus, Ohio, USA. 214 pp.

TAN L. AND VON FRESE R. R. B. (1997) Satellite geopotential modeling of the East Asian lithosphere (abstracts). *Eos Trans. AGU* **78(17)**, S114.

TANAKA K. L., SCOTT D. H. AND GREELEY R. (1992) Global stratigraphy. In *Mars* (eds. H. H. Kieffer, B. M. Jakosky, C. W. Snyder and M. S. Matthews), pp. 345–382. Univ. Arizona Press, Tucson, Arizona, USA.

VON FRESE R. R. B., HINZE W. J., BRAILE L. W. AND LUCA A. J. (1981) Spherical Earth gravity and magnetic anomaly modeling using Gauss–Legendre quadrature integration. *J. Geophys. Res.* **49**, 234–242.

VON FRESE R. R. B., KIM J. W. AND KIM J. (1997a) Analysis of anomaly correlations. *J. Geophys. Res.* **62**, 342–351.

VON FRESE R. R. B., TAN L., POTTS L. V., KIM J. W., MERRY C. L. AND BOSSLER J. D. (1997b) Lunar crustal analysis of Mare Orientale from topographic and gravity correlations. *J. Geophys. Res.* **102**, 25 657–25 676.

VON FRESE R. R. B., POTTS L. V., TAN L., KIM J. W., LEFTWICH T. W., MERRY C. J. AND BOSSLER J. D. (1998) Comparative crustal modeling of the Moon and Earth from topographic and gravity correlations (abstract). *Lunar Planet. Sci.* **29**, #1870, Lunar and Planetary Institute, Houston, Texas, USA (CD-ROM).

VON FRESE R. R. B., TAN L., KIM J. W. AND BENTLEY C. R. (1999) Antarctic crustal modeling from the spectral correlation of free-air gravity anomalies with terrain. *J. Geophys. Res.* **104**, 25 275–25 296.

WIECZOREK M. A. AND PHILLIPS R. J. (1999) Lunar multi-rings basins and the cratering process. *Icarus* **139**, 246–259.

WILHELMS D. E. (1987) *The Geologic History of the Moon*. U.S.G.S. Prof. Paper **1348**, U.S. Geol. Survey, Denver, Colorado, USA. 302 pp.

WILLIAMS K. K. AND ZUBER M. T. (1998) Re-evaluation of mare thicknesses based on lunar crater depth-diameter relationship. *Icarus* **103**, 1715–1724.

ZUBER M. T. *ET AL.* (2000) Internal structure and early thermal evolution of Mars from Mars Global Surveyor topography and gravity. *Science* **287**, 1788–1793.